nitude of this effect may be diminished when physisorbed water is present. Interactions between polymer OH groups and physisorbed water would be expected to be weaker and would be overcome at lower temperature than polymer OH/silanol interactions. On the basis of results presented here and previous results from Masia et al., it can be concluded that the catalytic and inhibitory effects of silica on the decomposition of PVB are dependent on polymer composition, atmospheric environment, and the surface characteristics of the silica. More work in this area is warranted to elucidate the details of these effects.

The primary degradation mechanisms of PVB lead to polymer residue unsaturation, which increases with increasing temperature. Because this unsaturation is highly conjugated, it is likely that large aromatic structures are formed on silica surfaces at high temperature. Subsequent carbonization of these species might leave regions in the silica in which carbon residue interferes with sintering. The result of this interference could be ceramic defects in the form of voids at locations where Si-O-C bonds were previously formed.

**Acknowledgment.** Support for this work from Hitachi, Ltd., is gratefully acknowledged.

# Liquid-Crystal Behavior in Ionic Complexes of Silver(I): Molecular Structure–Mesogenic Activity Relationship

M. Marcos, M. B. Ros, and J. L. Serrano*

*Química Orgánica, Instituto de Ciencia de Materiales de Aragón, Universidad de Zaragoza—C.S.I.C., 50009-Zaragoza, Spain*

M. A. Esteruelas, E. Sola, and L. A. Oro

*Química Inorgánica, Instituto de Ciencia de Materiales de Aragón, Universidad de Zaragoza—C.S.I.C., 50009-Zaragoza, Spain*

J. Barberá

*Laboratoire de Physique des Solides, Bâtiment 510, Université Paris-Sud, 91405 Orsay, France*

*Received July 12, 1990*

The liquid-crystal behavior of four series of ionic complexes of silver(I) with structure $[AgL_2]^+X^-$ have been investigated by using differential scanning calorimetry (DSC), optical microscopy, and X-ray diffraction techniques. Two different nonmesogenic pyridine derivatives, $NC_5H_4CH{=}NC_6H_4OC_nH_{2n+1}$ and $NC_5H_4COOC_6H_4OC_nH_{2n+1}$, were used as ligands (L) and four anions, $BF_4^-$, $CF_3SO_3^-$, $NO_3^-$, and $PF_6^-$, as counterions ($X^-$). The influence of both the organic ligand and counterion on the liquid-crystal properties of these complexes was studied. These complexes displayed mesogenic behavior identical with that exhibited by typical calamitic liquid crystals. Some of the complexes exhibited additional stable phases between the low-temperature solid phase and the liquid-crystalline phase. A comparative study has shown that pyridinecarboxylate derivatives show higher transition temperatures and wider mesophase ranges than similar imine derivatives. With regard to counterions, the less voluminous the anion, the broader the mesophase range and the lower the melting point.

## Introduction

Over the past few years numerous mesogenic molecules containing metals in their structure have been described. These compounds have the usual properties of liquid crystals, but also they can exhibit other special properties due to the presence of metals, as the mesophase allows an ordered distribution of the metal atoms and their electronic environment. As a result, new theoretical studies[1-4] and possible practical applications[5-10] are opening up for these compounds.

In general, the metallo mesogenic compounds described so far contain a liquid-crystal ligand. Recently we described the preparation of rhodium and iridium liquid-

(1) Marshall, K. L.; Jacobs, S. D. *Mol. Cryst. Liq. Cryst.* **1985**, *159*, 181.
(2) Giroud-Godquin, A. M.; Sigoud, G.; Achard M. F.; Hardouin, F. *J. Phys. Lett.* **1984**, *45*, L387. Giroud-Godquin, A. M.; Marchon, J. C.; Guillon, D.; Skoulios, A. *J. Phys. Chem.* **1986**, *90*, 5502.
(3) Piechocki, C.; Boulon, J. C.; Simon, J. *Mol. Cryst. Liq. Cryst.* **1987**, *149*, 115.
(4) Chandrasekhar, S.; Sadashiva, B. K.; Ratna, B. R.; Raja, N. V. *Pramana J. Phys.* **1988**, *30*, L491, and references therein.
(5) Ghedini, M.; Longeri, M.; Bartolino, R. *Mol. Cryst. Liq. Cryst.* **1982**, *84*, 207.
(6) Hunziker, M. Eur. Pat. Appl. Ed. 162,804 (Cl, C07D257/10), 1984.
(7) Matsushita Electric Industrial Co. Ltd. Jpn. Kokai Tokkyo Koho. Jp. 60 51,777 [85, 51,777] (Cl, C09K19/40).
(8) Bruce, D. W.; Dunmur, D. A.; Lalinde, E.; Maitlis, P. M.; Styring, P. *Nature (London)* **1986**, *323*, 791, and references therein.
(9) Bruce, D. W.; Lalinde, E.; Styring, P.; Dunmur, D. A.; Maitlis, P. M. *J. Chem. Soc., Chem. Commun.* **1986**, 581.
(10) Adams, H.; Bailey, N. A.; Bruce, D. W.; Dhillon, R.; Dunmur, D. A.; Hunt, S. E.; Lalinde, E.; Maggs, A. A.; Orr, R.; Styring, P.; Wragg, M. S.; Maitlis, P. M. *Polyhedron* **1988**, *7*, 1861.

0897-4756/90/2802-0748$02.50/0 

Chart I

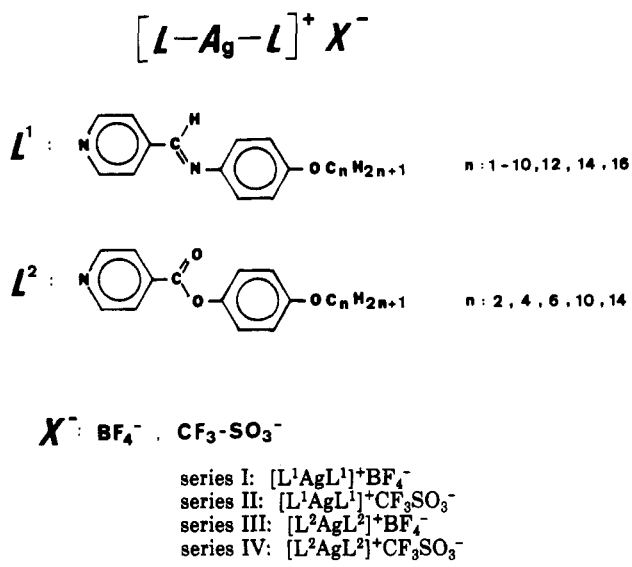


series I: $[L^1AgL^1]^+BF_4^-$
series II: $[L^1AgL^1]^+CF_3SO_3^-$
series III: $[L^2AgL^2]^+BF_4^-$
series IV: $[L^2AgL^2]^+CF_3SO_3^-$

crystal complexes of the type *cis*-$MCl(CO)_2(L^n)$ (M = Rh, Ir) formed by coordination of the nonmesomorphic organic ligand $L^n$ = $NC_5H_4CH{=}NC_6H_4OC_nH_{2n+1}$ to an organometallic fragment.[11] Using the same ligand, the complexes *trans*-$RhCl(CO)(L^n)_2$ formed by the reaction of $L^n$ with $RhCl(CO)_2(L^n)$ in presence of $ONMe_3$ showed high melting points and did not exhibit mesogenic behavior despite of their classical rodlike geometry.[12] We suggested that the strong intermolecular interactions in the solid state due to this favorable molecular geometry preclude mesophase formation. The different intermolecular interactions in an ionic crystal, compared with a covalent solid, could lead to a liquid-crystal behavior maintaining the rodlike shape of the molecule.

Most of the metallo mesogens already described are covalent materials, and only few examples of ionic metallo mesogens can be found in the literature.[8,13-15] Likewise, most of the studies developed to elucidate the molecular structure–mesogenic activity relationship concern only covalent materials,[16-19] and so the knowledge of ionic compound mesophases remains poor.

In this paper we present the synthesis of four new series of ionic silver complexes for which thermotropic liquid-crystal properties are also described; see Chart I.

The cation of these salts is formed by the coordination of two nonmesogenic pyridinic ligands to the silver atom in a linear geometry. The differences arising from the use of the two different kinds of ligand, 4-*n*-alkoxy-*N*-(4-pyridylmethylene)anilines ($L^1$) and 4-(4-*n*-alkoxyphenyl)pyridinecarboxylates ($L^2$), are investigated. The rodlike geometry of the cation is responsible for the liquid-crystal behavior. However, we also show that the mesogenic properties of the salts somehow depend on the counterion nature, so $BF_4^-$, $CF_3SO_3^-$, and also $NO_3^-$ and $PF_6^-$ salts have been investigated.

Table I. Analytical Data and Melting Points of Organic Ligands Used: $L^1$ = $NC_5H_4CH{=}NC_6H_4OC_nH_{2n+1}$; $L^2$ = $NC_5H_4COOC_6H_4OC_nH_{2n+1}$

| | | anal. found (calcd)[a] | | | |
|---|---|---|---|---|---|
| L | *n* | C | H | N | mp, °C |
| $L^1$ | 1 | 73.37 (73.33) | 5.76 (5.71) | 13.56 (13.20) | 98.7 |
| | 2 | 74.37 (74.30) | 6.47 (6.25) | 12.22 (12.38) | 96.7 |
| | 3 | 74.89 (74.96) | 6.89 (6.78) | 11.79 (11.66) | 93.6 |
| | 4 | 75.41 (75.55) | 7.37 (7.15) | 10.94 (11.02) | 74.3 |
| | 5 | 76.02 (76.07) | 7.41 (7.53) | 10.44 (10.44) | 66.1 |
| | 6 | 76.23 (76.55) | 8.04 (7.87) | 10.05 (9.92) | 58.7 |
| | 7 | 77.13 (76.97) | 8.31 (8.18) | 9.38 (9.45) | 68.4 |
| | 8 | 77.44 (77.36) | 8.66 (8.46) | 8.92 (9.02) | 65.4 |
| | 9 | 77.71 (77.66) | 8.74 (8.71) | 8.54 (8.63) | 71.5 |
| | 10 | 78.10 (78.05) | 8.80 (8.95) | 8.16 (8.28) | 69.1 |
| | 12 | 78.80 (78.62) | 9.44 (9.37) | 7.58 (7.64) | 76.7 |
| | 14 | 79.13 (79.12) | 9.57 (9.72) | 7.07 (7.10) | 81.6 |
| | 16 | 79.78 (79.55) | 10.48 (10.04) | 6.70 (6.63) | 87.0 |
| $L^2$ | 2 | 68.91 (69.14) | 5.01 (5.35) | 5.63 (5.76) | 94.7 |
| | 4 | 70.97 (70.85) | 6.57 (6.27) | 5.19 (5.17) | 75.4 |
| | 6 | 72.49 (72.24) | 7.91 (8.02) | 4.67 (4.68) | 54.5 |
| | 10 | 74.10 (74.36) | 8.53 (8.17) | 3.81 (3.94) | 87.7 |
| | 14 | 75.83 (75.91) | 9.19 (9.00) | 3.37 (3.40) | 94.8 |

[a] Analytical data in all table given in percent.

Table II. Analytical Data (Calculated Values in Parentheses) of Complexes $[AgL^1_2]^+BF_4^-$ (Series I)

| *n* | C | H | N |
|---|---|---|---|
| 1 | 50.59 (50.43) | 4.03 (3.90) | 9.03 (9.04) |
| 2 | 51.67 (51.96) | 4.64 (4.36) | 8.65 (8.65) |
| 3 | 52.59 (53.36) | 4.98 (4.77) | 7.82 (8.29) |
| 4 | 54.32 (54.64) | 5.05 (5.16) | 8.08 (7.90) |
| 5 | 55.48 (55.83) | 5.83 (5.51) | 7.63 (7.66) |
| 6 | 56.61 (56.93) | 5.94 (5.84) | 7.45 (7.37) |
| 7 | 57.83 (57.96) | 6.43 (6.14) | 7.01 (7.11) |
| 8 | 59.21 (58.90) | 7.01 (6.42) | 6.65 (6.86) |
| 9 | 59.46 (59.79) | 7.06 (6.69) | 6.47 (6.64) |
| 10 | 60.57 (60.62) | 7.38 (6.93) | 6.60 (6.42) |
| 12 | 61.99 (62.14) | 7.78 (7.38) | 6.07 (6.03) |
| 14 | 63.43 (63.48) | 8.24 (7.78) | 5.95 (5.69) |
| 16 | 64.35 (64.67) | 8.72 (8.14) | 5.45 (5.38) |

## Experimental Section

**(I) Synthesis. (a) Synthesis of the Ligands. 4-*n*-Alkoxy-*N*-(4-pyridylmethylene)anilines [$L^1$].** A mixture of 4-pyridinecarboxaldehyde (10 mmol), the respective 4-*n*-alkoxyaniline[20] (10 mmol), and a few drops of acetic acid in 30 mL of absolute ethanol as solvent was stirred at room temperature for 3 h. The Schiff bases that separated on cooling were filtered and washed with cold ethanol.

The products were purified by repeated recrystallizations from ethanol or hexane, yields 70–80%.

Elemental analysis and melting points of these compounds are gathered in Table I. All components of the series were satisfactorily characterized by IR and $^1H$ NMR techniques without significant differences within the series.

For *n* = 8: IR (Nujol) $\nu$ 1625, 1595, 1505, 1020, 830 $cm^{-1}$; $^1H$ NMR (200 MHz, $CDCl_3$) $\delta$ 0.87 (t, 3 H), 1.0–1.92 (m, 12 H), 3.95 (t, $J$ = 6 Hz, 2 H), 6.86 (d, $J$ = 9.6 Hz, 2 H), 7.26 (d, $J$ = 9.6 Hz, 2 H), 7.71 (d, $J$ = 5.1 Hz, 2 H), 8.40 (s, 1 H), 8.65 (d, $J$ = 5.1 Hz, 2 H).

**4′-*n*-Alkoxyphenyl 4-Pyridinecarboxylates [$L^2$].** *p*-*n*-Alkoxyphenol[20] (14 mmol) and $Et_3N$ (14 mmol) were dissolved

(11) Esteruelas, M. A.; Oro, L. A.; Sola, E.; Ros, M. B.; Serrano, J. L. *J. Chem. Soc., Chem. Commun.* **1989**, 55.
(12) Esteruelas, M. A.; Sola, E.; Oro, L. A.; Marcos, M.; Ros, M. B.; Serrano, J. L. *J. Organomet. Chem.* **1990**, *387*, 103.
(13) Markovitsi, D.; Bernard, M.; Andrê, J. J.; Simon, J. *J. Phys. Chem.* **1986**, *90*, 1323.
(14) Paleos, C. M.; Margomenou-Leonidopoulou, G.; Anastassopoulou, J. D.; Papaconstantinou, E. *Mol. Cryst. Liq. Cryst.* **1988**, *161*, 373.
(15) Bruce, D. W.; Dunmur, D. A.; Maitlis, P. M.; Styring, P.; Esteruelas, M. A.; Oro, L. A.; Ros, M. B.; Serrano, J. L.; Sola, E. *Chem. Mater.* **1989**, *1*, 479. Bruce, D. W., et al. Unpublished results.
(16) Barberá, J.; Espinet, P.; Lalinde, E.; Marcos, M.; Serrano, J. L. *Liq. Cryst.* **1987**, *2*, 833. Marcos, M.; Ros, M. B.; Serrano, J. L. *Liq. Cryst.* **1988**, *3*, 1129. Espinet, P.; Etxeberria, J.; Marcos, M.; Pérez, J.; Remón, A.; Serrano, J. L. *Angew. Chem., Int. Ed. Engl.* **1989**, *28*, 1065.
(17) Ghedini, M.; Armantano, S.; Bartolino, R.; Rustichelli, F.; Torquati, G.; Kirov, N.; Petrov, M. *Mol. Cryst. Liq. Cryst.* **1987**, *151*, 71.
(18) Ohta, K.; Ema, I.; Yamamoto, I.; Matsuzaki, K. *Liq. Cryst.* **1988**, *3*, 1671.
(19) Marcos, M.; Romero, P.; Serrano, J. L.; Bueno, C.; Cabeza, J. A.; Oro, L. A. *Mol. Cryst. Liq. Cryst.* **1989**, *167*, 123.
(20) Keller, P.; Liebert, L. *Solid. State Phys. Suppl.* **1986**, *14*, 19.

**Table III. Analytical Data (Calculated Values in Parentheses) of Complexes $[AgL^2_2]^+BF_4^-$ (Series III) and $[AgL^2_2]^+CF_3SO_3^-$ (Series IV)**

| $X^-$ | $n$ | C | H | N |
|---|---|---|---|---|
| $BF_4^-$ | 2 | 49.67 (49.37) | 3.82 (3.84) | 4.15 (4.11) |
| | 4 | 52.40 (52.13) | 4.65 (4.64) | 3.78 (3.80) |
| | 6 | 55.12 (54.49) | 5.62 (5.33) | 3.54 (3.53) |
| | 10 | 58.23 (58.35) | 6.73 (6.45) | 2.95 (3.09) |
| | 14 | 61.90 (61.36) | 7.99 (7.32) | 2.76 (2.75) |
| $CF_3SO_3^-$ | 4 | 50.39 (49.57) | 4.53 (4.28) | 3.41 (3.50) |
| | 6 | 51.89 (51.93) | 5.19 (4.95) | 3.15 (3.27) |
| | 10 | 55.80 (55.84) | 6.40 (6.04) | 2.79 (2.89) |
| | 14 | 58.98 (58.93) | 7.18 (6.90) | 2.53 (2.59) |

**Table IV. Analytical Data (Calculated Values in Parentheses) of Complexes $[AgL^1_2]^+CF_3SO_3^-$ (Series II)**

| $n$ | C | H | N |
|---|---|---|---|
| 5 | 52.84 (52.97) | 5.29 (5.08) | 6.98 (7.06) |
| 6 | 54.42 (54.08) | 5.75 (5.39) | 6.41 (6.81) |
| 7 | 55.43 (55.12) | 5.66 (5.69) | 6.63 (6.59) |
| 8 | 56.74 (56.09) | 6.12 (5.97) | 6.24 (6.38) |
| 9 | 57.69 (57.01) | 6.62 (6.23) | 5.92 (6.18) |
| 10 | 58.37 (57.87) | 6.80 (6.47) | 6.25 (6.00) |
| 12 | 59.91 (59.44) | 7.51 (6.92) | 5.35 (5.65) |
| 14 | 61.37 (60.85) | 8.02 (7.32) | 5.22 (5.35) |
| 16 | 62.21 (62.11) | 8.06 (7.68) | 4.98 (5.08) |

in 100 mL of $CH_2Cl_2$. 4-Picolinic acid chloride (14 mmol) was then added. The reaction mixture was stirred overnight at room temperature. The precipitate was filtered off, and the solvent was removed under reduced pressure. The residue was recrystallized several times from ethanol, yields 60–70%.

Elemental analysis and melting points of these compounds are gathered in Table I. All components of the series were satisfactorily characterized by IR and $^1H$ NMR techniques without significant differences within the series.

For $n$ = 14: IR (Nujol) $\nu$ 1735, 1592, 1510, 1256, 1187, 811 $cm^{-1}$; $^1H$ NMR (200 MHz, $CDCl_3$) $\delta$ 0.85 (t, 3 H), 1.0–1.87 (m, 24 H), 3.92 (t, $J$ = 6.4 Hz, 2 H), 6.85 (d, $J$ = 8.4 Hz, 2 H), 7.1 (d, $J$ = 8.4 Hz, 2 H), 7.9 (d, $J$ = 5.6 Hz, 2 H), 8.80 (d, $J$ = 5.6 Hz, 2 H).

**(b) Synthesis of the Complexes. Synthesis of $[AgL_2]^+BF_4^-$: Series I and III.** A solution of ligand L (2 equiv) and $AgBF_4$ (1 equiv) in ethanol was stirred in the dark under $N_2$ at room temperature for 20 min. The resulting suspension was concentrated under reduced pressure, filtered, washed with cold ethanol, and vacuum dried; yield about 75%.

The results of C, H, and N microanalysis of the complexes of these two series are gathered in Tables II and III. All components of the series were satisfactorily characterized by IR and $^1H$ NMR techniques without significant differences within the series.

For series I ($n$ = 8): IR (Nujol) $\nu$ 1624, 1588, 1501, 1242, 1130–1020 (br), 830 $cm^{-1}$; $^1H$ NMR (200 MHz, $CDCl_3$) $\delta$ 0.90 (m, 6 H), 1.13–1.87 (m, 24 H), 3.95 (t, $J$ = 6.5 Hz, 4 H), 6.87 (d, $J$ = 8.9 Hz, 4 H), 7.23 (d, $J$ = 8.9 Hz, 4 H), 7.79 (d, $J$ = 5.2 Hz, 4 H), 8.39 (s, 2 H), 8.74 (d, $J$ = 5.2 Hz, 4 H).

For series III ($n$ = 14): IR (Nujol) $\nu$ 1735, 1592, 1512, 1253, 1205, 1130–1050 (br), 818 $cm^{-1}$; $^1H$ NMR (200 MHz, $CDCl_3$) $\delta$ 0.88 (m, 6 H), 0.95–1.75 (m, 48 H), 3.95 (t, $J$ = 6.4 Hz, 4 H), 6.89 (d, $J$ = 9.0 Hz, 4 H), 7.08 (d, $J$ = 9.0 Hz, 4 H), 8.10 (d, $J$ = 6.2 Hz, 4 H), 8.94 (d, $J$ = 6.2 Hz, 4 H).

**Synthesis of $[AgL_2]^+CF_3SO_3^-$: Series II and IV.** A solution of ligand L (2 equiv) and silver triflate (1 equiv) in dry acetone stirred in the dark under $N_2$ at room temperature for 1 h led to a white suspension. The suspension was concentrated to 1 mL, and ether was added. The resulting white precipitate was filtered, washed with ether, and vacuum dried; yield about 90%.

The results of C, H, and N microanalysis of the complexes of these two series are gathered in Tables III and IV. All components of the series were satisfactorily characterized by IR and $^1H$ NMR techniques without significant differences within the series.

For series II ($n$ = 10): IR (Nujol) $\nu$ 1624, 1590, 1504, 1249, 1051, 833, 660 $cm^{-1}$; $^1H$ NMR (200 MHz, $CDCl_3$) $\delta$ 0.89 (m, 6 H), 1.00–1.90 (m, 32 H), 3.96 (t, $J$ = 6.6 Hz, 4 H), 6.85 (d, $J$ = 8.8 Hz, 4 H), 7.22 (d, $J$ = 8.8 Hz, 4 H), 7.80 (d, $J$ = 6.1 Hz, 4 H), 8.39 (s, 2 H), 8.82 (d, $J$ = 6.1 Hz, 4 H).

For series IV (4$n$ = 10): IR (Nujol) $\nu$ 1736, 1594, 1512, 1252, 1218, 818, 658 $cm^{-1}$; $^1H$ NMR (200 MHz, $CDCl_3$) $\delta$ 0.90 (m, 6 H), 0.91–1.80 (m, 32 H), 3.95 (t, $J$ = 6.3 Hz, 4 H), 6.94 (d, $J$ = 9.0 Hz, 4 H), 7.08 (d, $J$ = 9.0 Hz, 4 H), 8.12 (d, $J$ = 6.1 Hz, 4 H), 8.98 (d, $J$ = 6.1 Hz, 4 H).

**Synthesis of $[AgL^1_2]^+NO_3^-$ with $n$ = 8.** 4-($n$-Octyloxy)-$N$-(4-pyridylmethylene)aniline (2 equiv) and silver nitrate (1 equiv) were stirred in ethanol at room temperature for 2 h in the dark under $N_2$. The resulting yellow suspension was concentrated under reduced pressure, filtered, washed with cold ethanol, and vacuum dried, yield 61%. IR (Nujol) $\nu$ 1620, 1588, 1506, 1380–1300 (br), 1255, 1024, 836 $cm^{-1}$; $^1H$ NMR (200 MHz, $CDCl_3$) $\delta$ 0.89 (m, 6 H), 1.00–1.83 (m, 24 H), 3.96 (t, $J$ = 6.5 Hz, 4 H), 6.89 (d, $J$ = 8.9 Hz, 4 H), 7.27 (d, $J$ = 8.9 Hz, 4 H), 7.81 (d, $J$ = 5.9 Hz, 4 H), 8.44 (s, 2 H), 8.73 (d, $J$ = 5.9 Hz, 4 H).

Analytical data (calculated values in parentheses): C, 60.22 (60.75); H, 6.69 (6.63); N, 8.84 (8.85).

**Synthesis of $[AgL^1_2]^+PF_6^-$ with $n$ = 8.** An ethanolic suspension of 4-($n$-octyloxy)-$N$-(4-pyridylmethylene)aniline (2 equiv) was added to a suspension containing 1 equiv of $AgNO_3$ and 2 equiv of ammonium hexafluorophosphate.

The resulting suspension was stirred for 2 h, and the yellow solid obtained was filtered, washed with ethanol, and vacuum dried, yield 82%. IR (Nujol) $\nu$ 1621, 1587, 1504, 1251, 1020, 855, 837 $cm^{-1}$; $^1H$ NMR (200 MHz, $CDCl_3$) $\delta$ 0.89 (m, 6 H), 1.00–1.83 (m, 24 H), 3.98 (t, $J$ = 6.5 Hz, 4 H), 6.95 (d, $J$ = 8.9 Hz, 4 H), 7.27 (d, $J$ = 8.9 Hz, 4 H), 7.79 (d, $J$ = 5.9 Hz, 4 H), 8.49 (s, 2 H), 8.74 (d, $J$ = 5.9 Hz, 4 H).

Analytical data (calculated values in parentheses): C, 54.37 (54399); H, 6.27 (5.99); N. 6.31 (6.41).

**(II) Techniques.** Elemental analyses were performed with a Perkin-Elmer 240 B microanalyzer. $^1H$ NMR spectra were recorded on a Varian XL-200 spectrometer. IR spectra were obtained on a Perkin-Elmer 599 spectrometer. Melting points of ligands were measured by using a Mettler FP61 apparatus.

The textures of the mesophases were studied with a Meiji polarizing microscope equipped with a Mettler PF82 hot stage and FP80 central processor.

Transition temperatures were measured by differential scanning calorimetry with a Perkin-Elmer DSC-2 and DSC-7 operated at a scanning rate of 10°/min. The apparatus were calibrated with indium (429.6 K, 28.4 J/g) as standard.

X-ray diffraction experiments were carried out using a monochromatic Cu K$\alpha$ X-ray beam issued from a double bent pyrolitic graphite monochromator. The samples, held in a Lindemann glass tube (0.5-mm o.d.) were aligned by a magnetic field perpendicular to the X-beam. The temperature of the sample was constant within ±1 K. The diffraction pattern was recorded on a photographic film.

## Results and Discussion

**Mesogenic Behavior.** Most of the complexes here described form liquid crystals. These four series show mesogenic behavior identical with that observed in classical rodlike organic compounds: the longer the terminal chain, the lower melting points and the more ordered liquid-crystal phases. The transition temperatures and enthalpy data of the compounds of these four series are gathered in Tables V–VIII and Figures 1–4. We observed that many of these complexes decompose once they had become isotropic. For this reason first DSC cycle data were used for all the silver complexes here described.

As can be seen, most of the complexes show smectic phases, and only the ethoxy derivative of series I shows a nematic phase.

**Characterization of the Mesophases.** The identity of the mesophases exhibited by these silver complexes has been assigned on the basis of optical textures.[21]

(21) (a) Demus, D.; Ritcher, L. *Textures of Liquid Crystals*; V.E.B. Deutscher Verlag fur Grundtoffindustrie, 1978. (b) Gray, G. W.; Goodby, J. W. G. *Smectic liquid crystals: Textures and structures*; Leonard Hill: 1984.

**Table V. Optical, Thermal, and Thermodynamic Data of Complexes $[AgL^1_2]^+BF_4^-$ (Series I)**

| *n* | transition[a] | temp,[b] °C | $\Delta H$,[b] kJ/mol |
|---|---|---|---|
| 1 | C-I | 225.3 | 35.9 |
| 2 | C-N | 194.9 | 41.8 |
| | N-I | 223.8 | 1.4 |
| 3 | C-$S_A$ | 175.1 | 25.7 |
| | $S_A$-I | 190.7 | 0.2 |
| 4 | C-C′ | 146.3 | 19.5 |
| | C′-$S_A$ | 163.1 | 19.4 |
| | $S_A$-I | 188.8 | 0.2 |
| 5 | C-C′ | 93.9 | 7.3 |
| | C′-C″ | 130.3 | 12.4 |
| | C″-$S_A$ | 136.7 | 9.3 |
| | $S_A$-I | 209.5 | 0.9 |
| 6 | C-C′ | 98.3 | 20.3 |
| | C′-$S_A$ | 131.8 | 19.8 |
| | $S_A$-I[c] | 201[d] (dec) | |
| 7 | C-C′ | 95.7 | 1.5 |
| | C′-$S_A$ | 126.6 | 18.1 |
| | $S_A$-I[c] | 210[d] (dec) | |
| | $S_A$-$S_C$[c] | 88[d,e] | |
| 8 | C-C′ | 96.9 | 25.7 |
| | C′-C″ | 106.1 | 2.2 |
| | C″-$S_C$ | 114.4 | 16.8 |
| | $S_C$-$S_A$[c] | 168[d] | |
| | $S_A$-I[c] | 202[d] (dec) | |
| 9 | C-C′ | 79.6 | 33.0 |
| | C′-$S_C$ | 107.0 | 11.3 |
| | $S_C$-$S_A$[c] | 181[d] | |
| | $S_A$-I[c] | 210[d] (dec) | |
| 10 | C-C′ | 87.6 | 51.5 |
| | C′-$S_C$ | 102.8 | 10.1 |
| | $S_C$-$S_A$[c] | 188[d] | |
| | $S_A$-I[c] | 206[d] (dec) | |
| 12 | C-C′ | 85.6 | 60.3 |
| | C′-$S_C$ | 103.7 | 10.0 |
| | $S_C$-$S_A$[c] | 195[d] | |
| | $S_A$-I[c] | 211[d] (dec) | |
| 14 | C-C′ | 83.7 | ] 57.1[f] |
| | C′-$S_C$ | 88.2 | |
| | $S_C$-$S_A$[c] | 186[d] | |
| | $S_A$-I[c] | 208[d] (dec) | |
| 16 | C-$S_1$[g] | 88.1 | 67.0 |
| | $S_1$-$S_C$ | 98.6 | 6.6 |
| | $S_C$-$S_A$[c] | 194[d] | |
| | $S_A$-I[c] | 217[d] (dec) | |

[a] C, crystal; N, nematic; S, smectic; I, isotropic liquid. [b] Data referred to the first DSC cycle. Temperature data as peak onset. [c] Not detected by DSC. [d] Optical microscopic data. [e] Monotropic transition. [f] Combined enthalpies. [g] Unidentified mesophase.

The nematic phase observed in one of these compounds showed the typical Schlieren texture with the characteristic two- or four-brush isogyres. The $S_A$ phase present in all mesogenic compounds studied was identified by the appearance on heating of both mielinic and homeotropic textures without subjecting the sample under mechanical stress. The tendency of these silver complexes to give rise to homeotropic texture is noteworthy. In some cases a focal conic texture could be observed on cooling. The $S_C$ mesophase was mainly identified by the appearance of Schlieren textures on both heating and cooling.

We were unable to identify the other phases, called by us as $S_1$, $S_2$, and $S_3$ (Tables V, VII, and VIII) exhibited by these complexes. These phases were much more viscous than the N, $S_A$, and $S_C$ phases, whose viscosities were similar to that observed in classical calamitic organic liquid crystals. Even though all the transitions involving these unidentified phases were clearly detected by DSC, some of them were not easily observed by microscopy. Thus, no clear texture change was observed for the $S_1$–$S_C$ transition in $BF_4^-$ imino complex with $n = 16$, either on heating or cooling. However, a clear viscosity change was observed under mechanical stress. With regard to $S_2$ and $S_3$ phases

**Table VI. Optical, Thermal, and Thermodynamic Data of Complexes $[AgL^1_2]^+CF_3SO_3^-$ (Series II)**

| *n* | transition[a] | temp,[b] °C | $\Delta H$,[b] kJ/mol |
|---|---|---|---|
| 5 | C-I | 163.7 | 40.1 |
| 6 | C-I | 177.6 | 54.9 |
| | I-$S_A$[e] | 146.6 | 1.5 |
| 7 | C-I | 165.5 | 53.2 |
| | I-$S_A$[e] | 162.3 | 4.3 |
| 8 | C-$S_A$ | 153.7 | 44.5 |
| | $S_A$-I | 173.4 | 5.4 |
| 9 | C-$S_A$ | 145.0 | 45.9 |
| | $S_A$-I | 176.5 | 5.6 |
| 10 | C-C′ | 85.7 | 5.1 |
| | C′-$S_A$ | 142.1 | 48.9 |
| | $S_A$-I | 183.4 | 5.5 |
| 12 | C-$S_A$ | 133.9 | 58.0 |
| | $S_A$-I | 187.6 | 3.8 |
| | $S_A$-$S_C$[c,e] | 122[d] | |
| 14 | C-$S_C$ | 128.3 | 53.6 |
| | $S_C$-$S_A$[e] | 142[d] | |
| | $S_A$-I | 185.4 | 3.2 |
| 16 | C-$S_C$ | 126.6 | 101.2 |
| | $S_C$-$S_A$[c] | 151[d] | |
| | $S_A$-I | 188.2 | 3.3 |

[a] C, crystal; S, smectic; I, isotropic liquid. [b] Data referred to the first DSC cycle. Temperature data as peak onset. [c] Not detected by DSC. [d] Optical microscopic data. [e] Monotropic transition.

**Table VII. Optical, Thermal, and Thermodynamic Data of Complexes $[AgL^2_2]^+BF_4^-$ (Series III)**

| *n* | transition[a] | temp,[b] °C | $\Delta H$,[b] kJ/mol |
|---|---|---|---|
| 2 | C-$S_A$ | 216.2 | 48.3 |
| | $S_A$-I | 235.7 | 5.5 |
| 4 | C-C′ | 110.5 | 15.7 |
| | C′-$S_A$ | 172.9 | 20.3 |
| | $S_A$-I | 257.5 | 11.7 |
| 6 | C-$S_A$ | 160.9 | 67.6 |
| | $S_A$-I | 261.7 | 15.3 |
| | $S_A$-$S_C$[c,e] | 152[d] | |
| 10 | C-$S_2$[f] | 63.7 | 63.3 |
| | $S_2$-$S_C$ | 161.8 | 45.9 |
| | $S_C$-$S_A$[c] | 203[d] | |
| | $S_A$-I[c] | 217[d] | |
| 14 | C-$S_2$ | 82.1 | 89.5 |
| | $S_2$-$S_C$ | 159.8 | 38.4 |
| | $S_C$-$S_A$[c] | 215[d] | |
| | $S_A$-I | 260.7 | 16.3 |

[a] C, crystal; S, smectic; I, isotropic liquid. [b] Data referred to the first DSC cycle. Temperature data as peak onset. [c] Not detected by DSC. [d] Optical microscopic data. [e] Monotropic transition. [f] Unidentified mesophase.

**Table VIII. Optical, Thermal, and Thermodynamic Data of Complexes $[AgL^2_2]^+CF_3SO_3^-$ (Series IV)**

| *n* | transition[a] | temp,[b] °C | $\Delta H$,[b] kJ/mol |
|---|---|---|---|
| 4 | C-I | 183.3 | 58.8 |
| 6 | C-$S_A$ | 152.4 | 51.3 |
| | $S_A$-I | 155.0 | 3.4 |
| 10 | C-$S_3$[c] | 110.9 | 24.4 |
| | $S_3$-$S_2$[c] | 124.3 | 10.1 |
| | $S_2$-$S_A$ | 142.6 | 20.9 |
| | $S_A$-I | 181.0 | 5.3 |
| 14 | C-$S_3$ | 105.4 | 56.6 |
| | $S_3$-$S_2$ | 113.6 | 7.5 |
| | $S_2$-$S_A$ | 138.7 | 31.1 |
| | $S_A$-I | 184.4 | 7.3 |

[a] C, crystal; S, smectic; I, isotropic liquid. [b] Data referred to the first DSC cycle. Temperature data as peak onset. [c] Unidentified mesophase.

detected in compounds of series IV, the first phase that appeared on heating ($S_3$) showed the texture shown in Figure 5.

However, no texture change was observed on transition

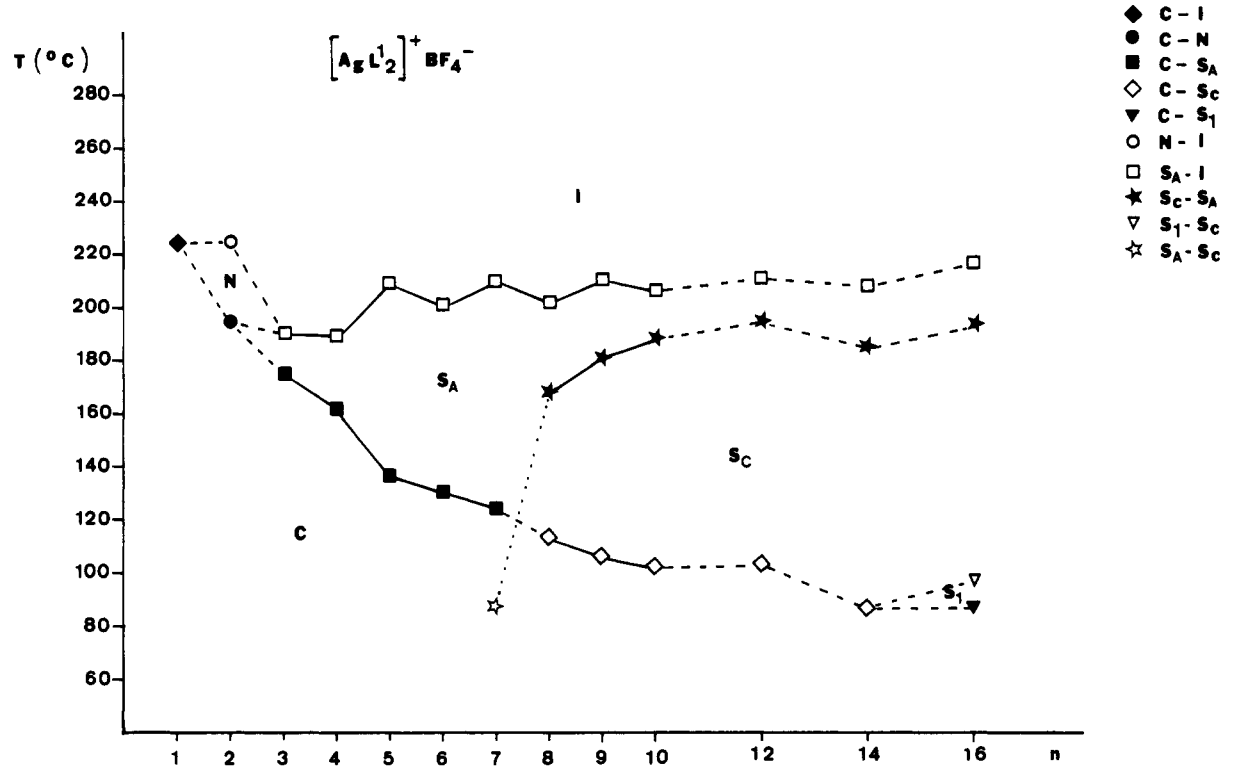


**Figure 1.** Transition temperatures as a function of alkyl chain length for compounds of series I: $[AgL^1_2]^+BF_4^-$.

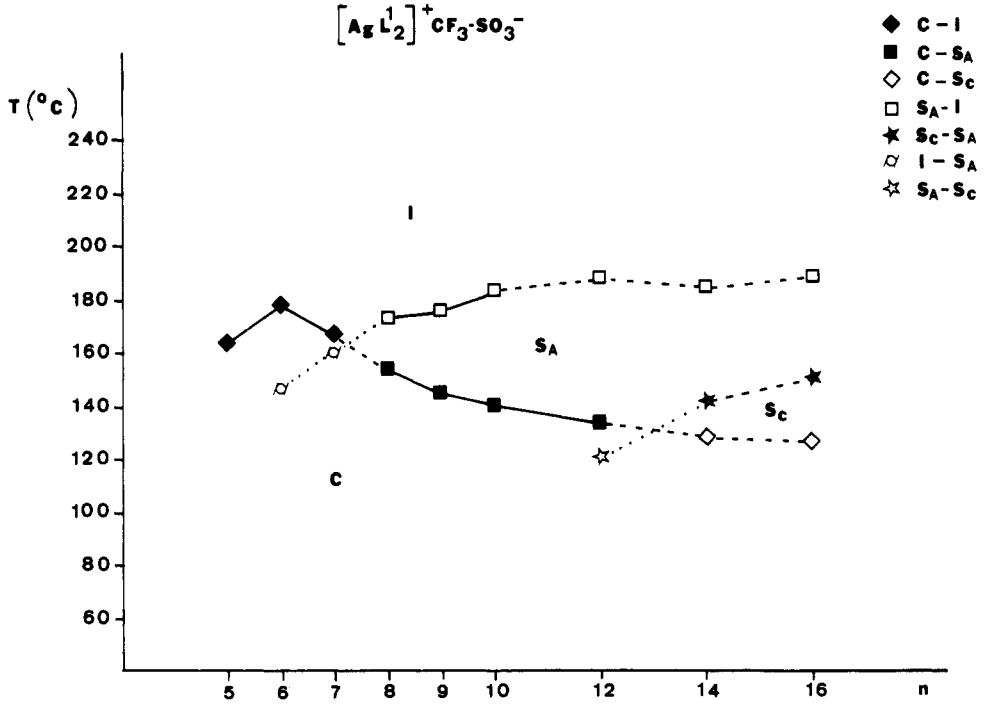


**Figure 2.** Transition temperatures as a function of alkyl chain length for compounds of series II: $[AgL^1_2]^+CF_3SO_3^-$.

to the other phase, namely $S_2$, on heating. Nevertheless a clear $S_2$–$S_3$ transition was detected on cooling. A photographic sequence of the cooling of compound $[AgL^2_2]^+CF_3SO_3^-$ with $n = 10$ is shown in Figures 6–8. Figure 6 shows the transition from the homeotropic $S_A$ phase to $S_2$ phase. Figure 7 shows the characteristic texture of the $S_2$ phase. This texture clearly changed to the different texture of the phase $S_3$ as shown in Figure 8. Once the texture shown in Figure 8 was obtained, the $S_3$–$S_2$ transition could be observed on heating. Both $S_2$ and $S_3$ mesophases were very viscous, and the viscosity changed drastically when the transition to $S_A$ took place. The phase previous to $S_C$ observed for the compounds in series III showed a texture similar to the one shown in Figure 5, and it could be considered as a $S_2$ phase.

The repetitivity of the textures and the transition temperatures observed by microscope and DSC in different cycles carried out below the clearing point and the fact that when pressure is applied the glass slide and the cover slip can be made to glide over one another during the optical observation indicate that these phases are no typical crystals but so-called "crystalline phases".[21b,22] Unfortu-

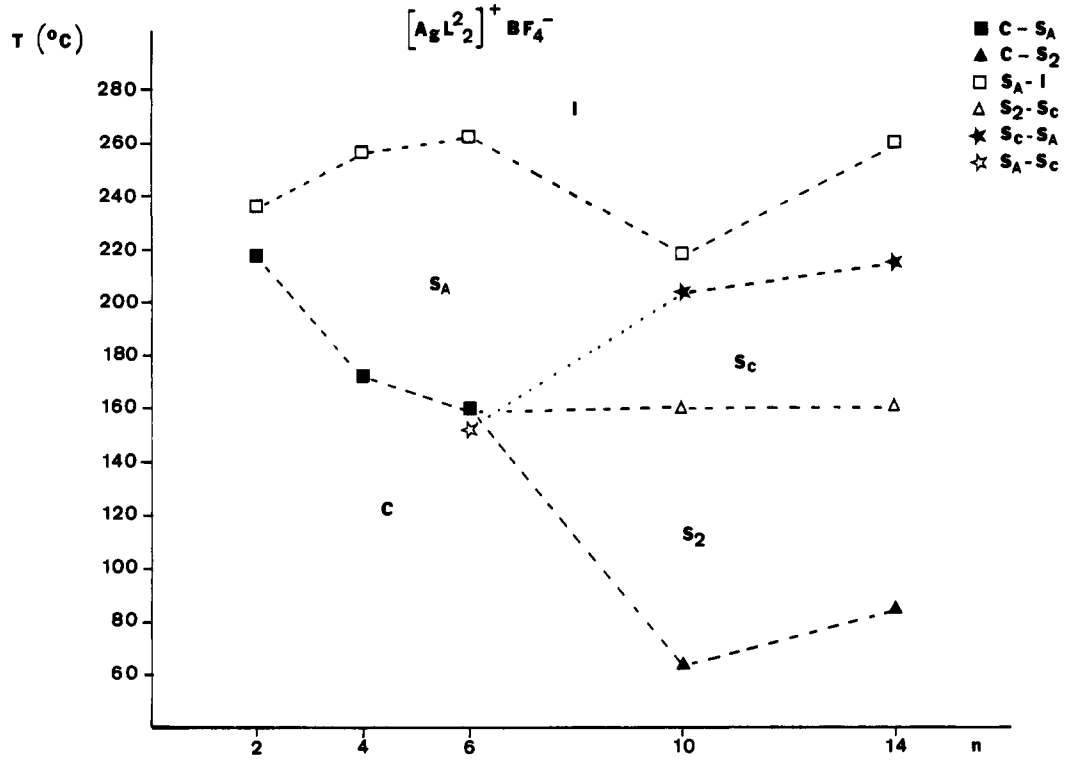


**Figure 3.** Transition temperatures as a function of alkyl chain length for compounds of series III: $[AgL^2_2]^+BF_4^-$.

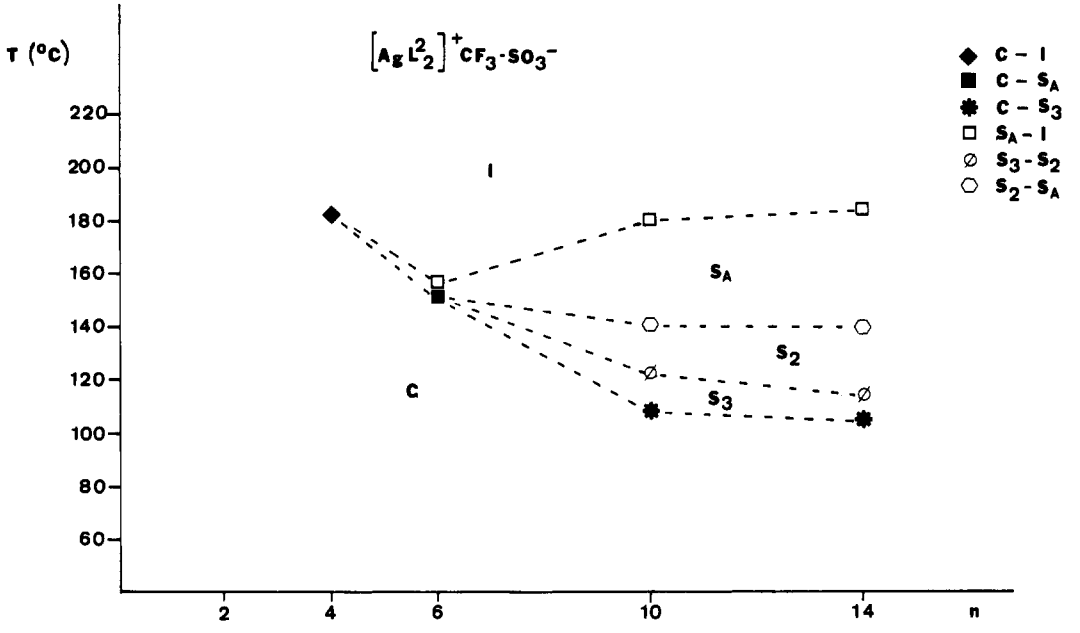


**Figure 4.** Transition temperatures as a function of alkyl chain length for compounds of series IV: $[AgL^2_2]^+CF_3SO_3^-$.

nately, the X-ray instability of these compounds did not allow us to obtain more conclusive data.

The studies under the microscope also showed that practically all these silver complexes decompose at the clearing point or, even in some cases, a slow decomposition had already started several degrees below this transition. However, for many of these compounds, a clear transition to isotropic liquid were detected by DSC that also appeared in following scannings (see Figure 9). These differences in thermal behavior, depending on the technique used, could be due to the negative effect of both air and light (not present in calorimetric measurements) on silver complexes.

**Influence of the Ligand on the Mesogenic Properties.** As expected, the modifications introduced in the pyridine ligand led to important changes in the liquid-crystal properties of the silver complexes, which will be commented on below. However, it is noteworthy that while series I and II derived from $L^1$ show a similar tendency (see Figures 1 and 2), more significant differences are observed between the two ester series (III and IV; see Figures 3 and 4).

Figures 10 and 11 show a comparative study of the mesomorphic properties of the silver complexes describes in terms of the organic ligand.

(22) Pershan, P. S. *Structure of Liquid Crystal Phases*; World Scientific Lecture Notes in Physics, World Scientific, 1988; Vol. 23.

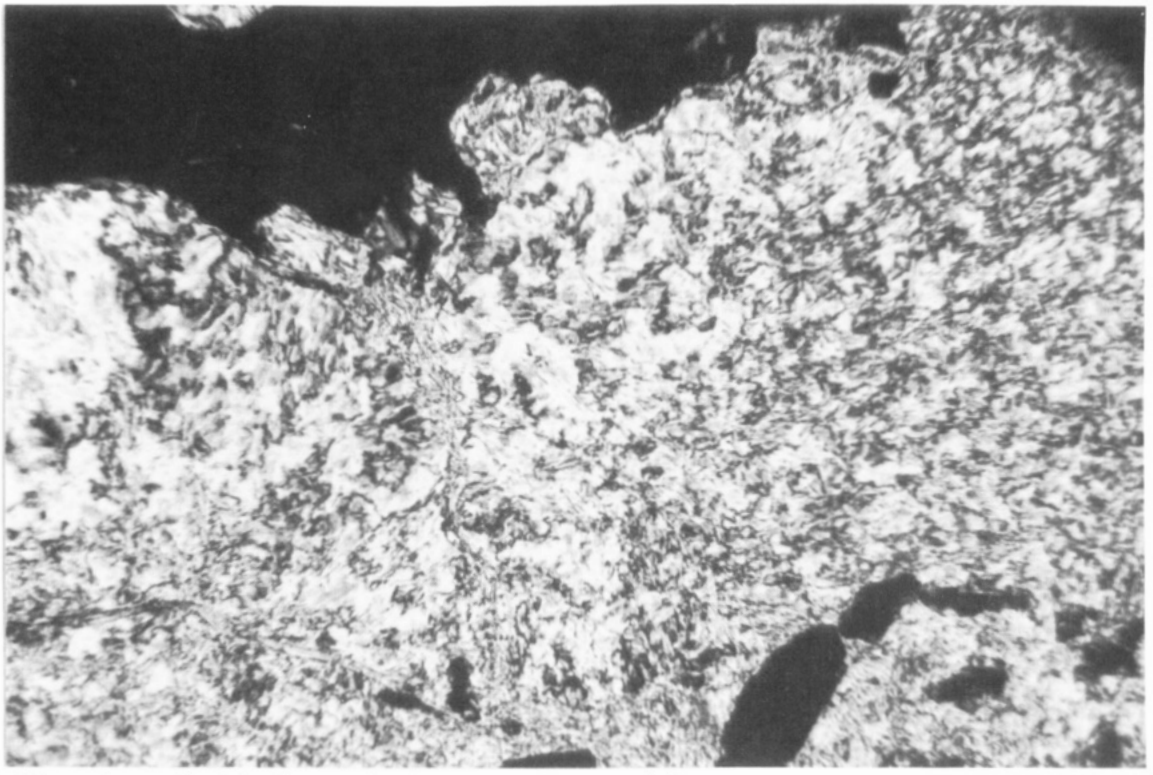

**Figure 5.** Photomicrograph of $S_2$ phase on heating at 127 °C of $[AgL^2_2]^+CF_3SO_3^-$ ($n$ = 10) viewed between crossed polarizers.

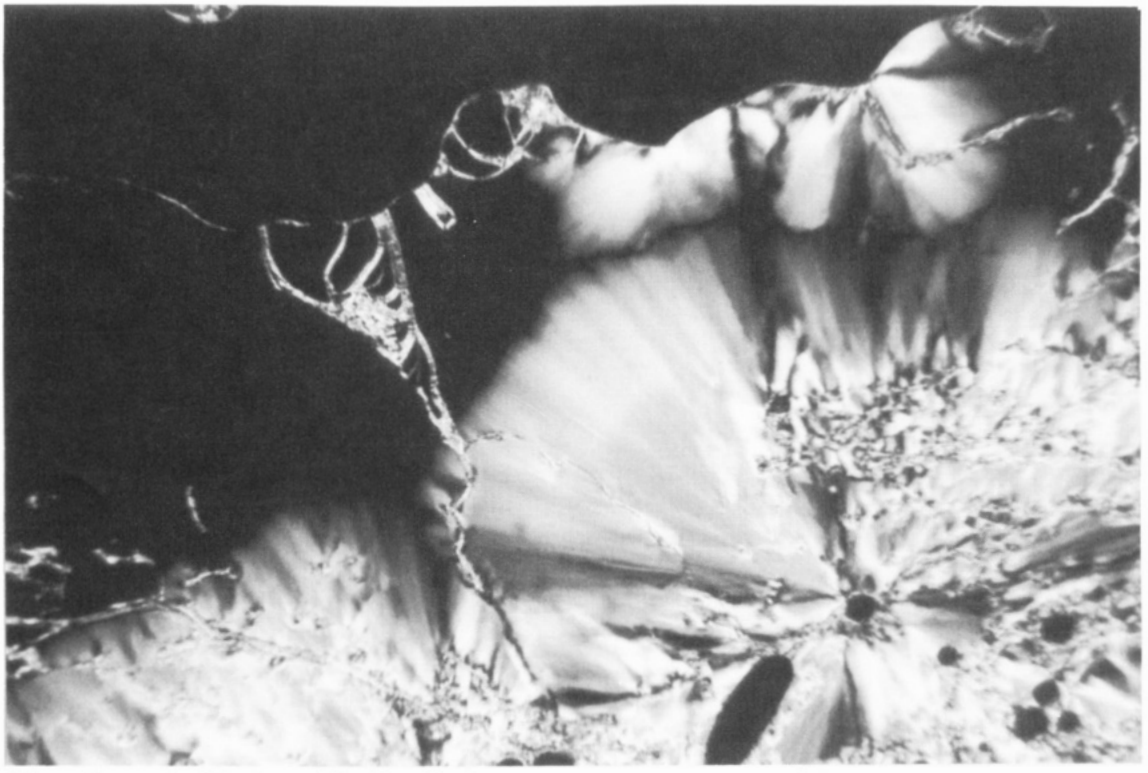

**Figure 6.** Photomicrograph of $S_2$ phase arising from $S_A$ phase on cooling at 139 °C of $[AgL^2_2]^+CF_3SO_3^-$ ($n$ = 10) viewed between crossed polarizers.

As can be seen, for the same anion, similar chain lengths are needed to get mesomorphism, but the ester complexes exhibit better liquid-crystal properties than the imine compounds. Pyridinecarboxylate derivatives show wider mesophase ranges as well as richer phase polymorphism than the imine compounds. As far as the stability of the mesophases is concerned, in $CF_3SO_3^-$ derivatives both ligands stabilize the mesophase in a similar way, whereas higher mesophase isotropic liquid transition temperatures were observed in $BF_4^-$ ester derivatives. These properties differ slightly from that observed in classical organic rodlike imine and ester liquid crystals,[23] indicating the role that the longer structure of these molecules and the

(23) Demus, D.; Demus, H.; Zaschke, H. *Flussige Kristalle in Tabellen I*; V.E.B. Deutscher Verlag Grundtoffindustrie, 1976. Demus, D.; Zaschke, H. *Flussige Kristalle in Tabellen II*; V.E.B. Deutscher Verlag Grundtoffindustrie, 1984.

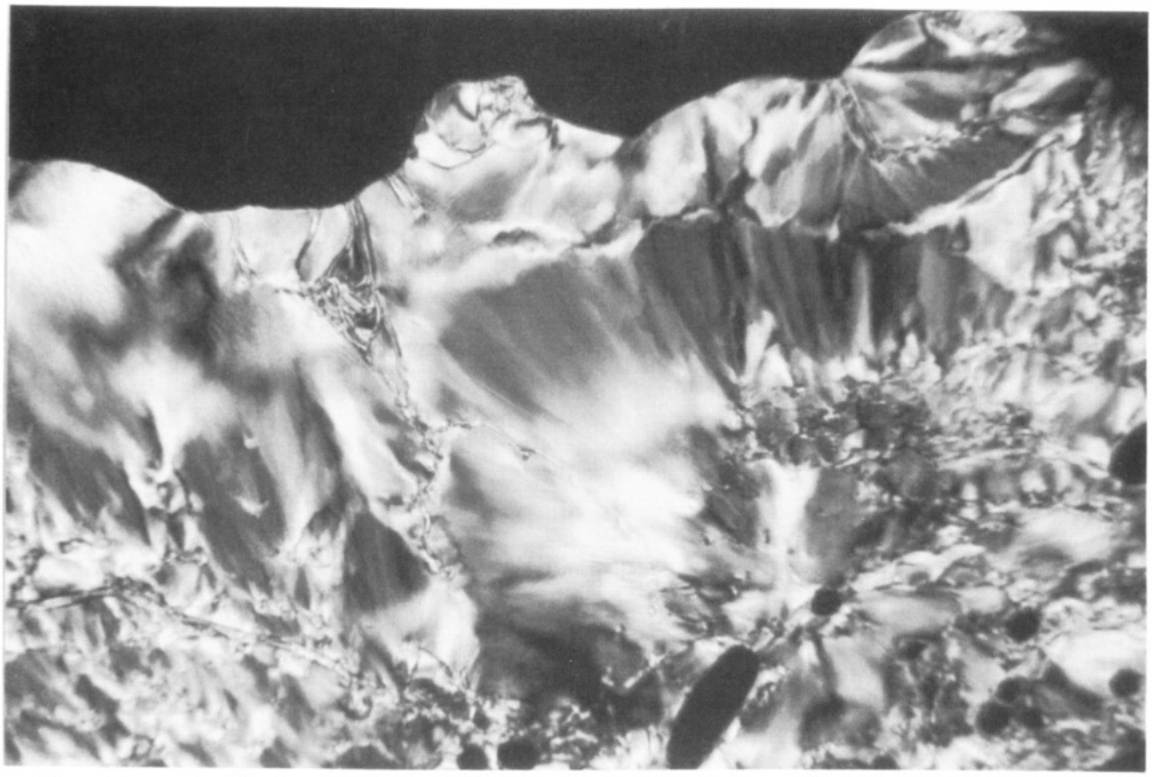

**Figure 7.** Photomicrograph of $S_3$ phase arising from $S_2$ phase on cooling at 121 °C of $[AgL^2_2]^+CF_3SO_3^-$ ($n$ = 10) viewed between crossed polarizers.

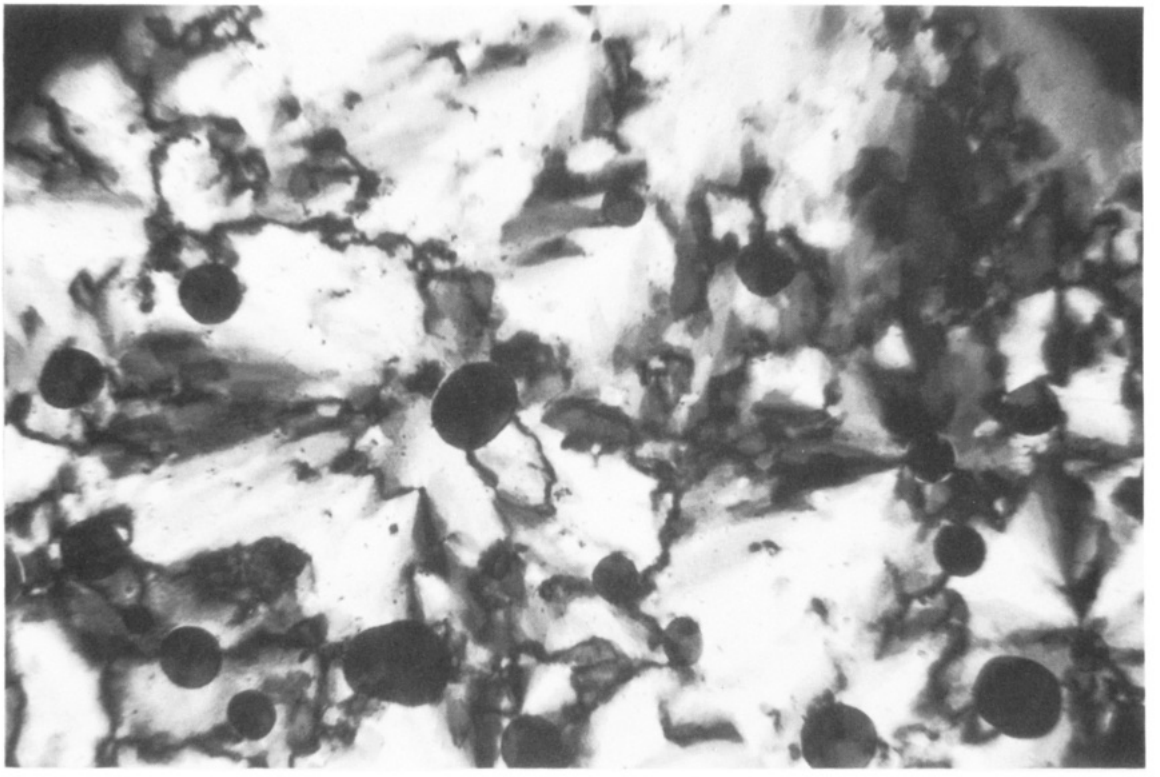

**Figure 8.** Photomicrograph of $S_3$ phase on cooling at 110 °C of $[AgL^2_2]^+CF_3SO_3^-$ ($n$ = 10) viewed between crossed polarizers.

characteristics of the anion influence the mesomorphic behavior of this kind of compound.

It is noteworthy that only one of the complexes in these four series shows nematic phase $[AgL^1_2]^+BF_4^-$ ($n$ = 2), while similar $CF_3SO_3^-$ stilbazol complexes of silver reported in the literature exhibit nematic phase.[15] This may well due to the higher planarity of stilbazol ligands. X-ray data obtained for the crystal structure of the *trans*-stilbene[24] indicate that these substances are nearly planar; however, benzylideneanilines and phenyl benzoates are not planar. For these latter compounds the two aromatic rings form an angle about of 17–45°[25] and 55–90°[26] to each other,

(24) Robertson, J. M.; Woodward, I. *Proc. R. Soc., Ser. A* **1937**, *162A*, 568. Young, W. R.; Aviram, A.; Cox, R. J. *J. Am. Chem. Soc.* **1972**, *94*, 3976.

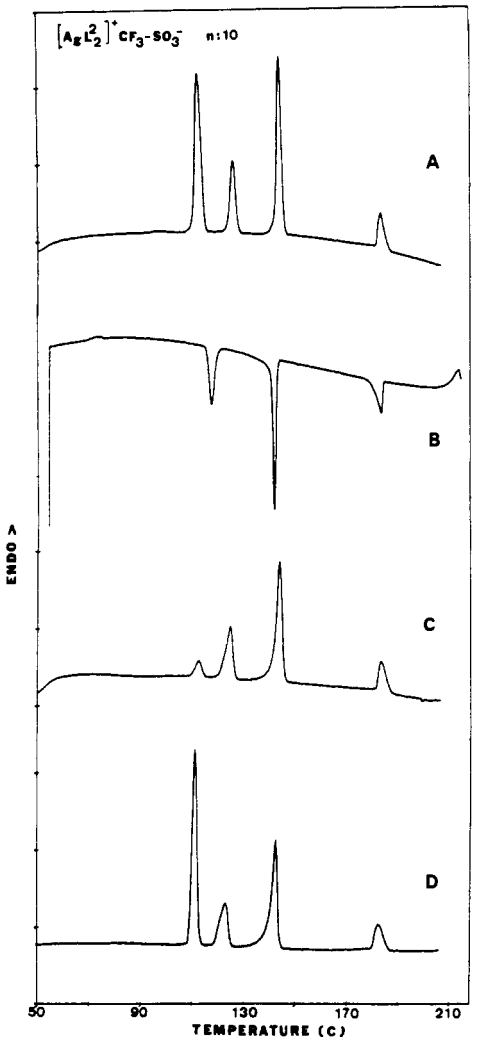


**Figure 9.** DSC thermograms of the complex $[AgL^2_2]^+CF_3SO_3^-$ ($n$ = 10): (A and B) first heating and cooling cycles; (C) second heating cycle [3 h after cycle B]; (D) third heating cycle [24 h after cycle C]. Scanning rate 10 °C/min.

respectively, depending on the 4,4′ substituents. The greater planarity of stilbazol ligands allows them to form liquid crystals by themselves,[27] which does not happen with the imino and ester ligands. For the stilbazol complexes, the more planar organic part allows nematic arrangement above 200 °C before clearing, while the imine and ester ligands, whose complexes form an isotropic liquid at even lower temperatures, do not.

**Influence of the Counterion on the Mesogenic Properties.** A comparative study of the four silver complex series reveals that $BF_4^-$ compounds have the best mesogenic properties. Practically all the members of series I and III exhibit liquid-crystal behavior, while a longer terminal chain ($n$ = 6) is needed to get mesomorphism with $CF_3SO_3^-$ as the anion. With regard to the melting points, $BF_4^-$ complexes always melt at lower temperatures than their homologues in the $CF_3SO_3^-$ series, and likewise $BF_4^-$

**Table IX. Optical, Thermal, and Thermodynamic Data of Complexes $[AgL^1_2]^+X^-$ with $n$ = 8**

| $X^-$ | transition[a] | temp,[b] °C | $\Delta H$,[b] kJ/mol |
|---|---|---|---|
| $NO_3^-$ | C-C′ | 75.7 | |
| | C′-C″ | 80.8 | 33.1[c] |
| | C″-$S_C$ | 84.2 | |
| | $S_C$-$S_A$[d] | 154[e] | |
| | dec | 186 | |
| $PF_6^-$ | C-$S_A$ | 192.1 | 69.6 |
| | $S_A$-I | 241.6 | 10.9 |

[a] C, crystal; S, smectic; I, isotropic liquid. [b] Data referred to the first DSC cycle. Temperature data as peak onset. [c] Combined enthalpies. [d] Not detected by DSC. [e] Optical microscope data.

silver complexes exhibit the widest mesophase ranges, showing smectic polymorphism at shorter chain length than the $CF_3SO_3^-$ derivatives. As was mentioned above, the $CF_3SO_3^-$ anion stabilizes the $S_A$ phase less than $BF_4^-$ anion, regardless of the ligand. However, the $BF_4^-$ ester complexes exhibit very high clearing points. This result seems to indicate that the counterion somehow conditions the influence of the ligand.

To know more about the influence of the anion on the mesomorphic beavior of these silver complexes, two new (octyloxy)imine derivatives with $NO_3^-$ and $PF_6^-$ as anion were synthesized and studied (Table IX).

The four counterions used, $BF_4^-$, $CF_3SO_3^-$, $NO_3^-$, and $PF_6^-$, have different geometrical structures and volumes[28] as shown in the sequence

$$NO_3^- < BF_4^- < PF_6^- < CF_3SO_3^-$$

This should allow different cation–cation approximations and determination of the consequent molecular interactions that determine mesogenic behavior.

In Figure 12 the liquid-crystal properties of these different (octyloxy)imine derivatives are represented.

As can be seen, the small planar anion $NO_3^-$ gives rise to the lowest melting point, the widest mesophase ranges as well as two smectic phases whereas the (octyloxy)-imine–silver complex with $CF_3SO_3^-$ anion shows the shortest mesophase range, only of type $S_A$. The intermediate spherical counterions $BF_4^-$ and $PF_6^-$ exhibit intermediate properties. Thus, the $BF_4^-$ complex shows (as does the $NO_3^-$ complex) a low melting point and a broad polymorphic mesophase range, while the $PF_6^-$ complex melts at a very high temperature and also exhibits a short mesophase range only of type $S_A$. The noticeably different structural characteristics of the $CF_3SO_3^-$ ion also seem to influence the molecular arrangement of the solid phase of this complex, giving rise to a lower melting point than the $PF_6^-$ complex.

Generally with these compounds, the smaller the volume of the counterion, the broader the mesophase range and the lower the melting point. When the counterion is sufficiently small to allow a molecular arrangement to be retained after melting, the apparently strong interactions (high melting points) of the solid state are broken, and the melting points decrease to give rise to mesophases that are more ordered than $S_A$. Thus, in ionic silver complexes of this kind the linear geometry of the cation group, typical of rodlike compounds, increases intermolecular interactions and allows a regular arrangement of the molecules, which favors mesomorphism. The counterion, probably located near the silver atom, where the positive charge is most likely to be concentrated, determines intermolecular distances having, its size being a considerably influence on

(25) Burgi, H. B.; Dunitz, J. D. *Helv. Chim. Acta* **1970**, *53*, 1747. Bernstein, I.; Izak, I. *J. Chem. Soc., Perkin Trans. 2* **1976**, 429. Van, G. V.; Vijayan, K. *Mol. Cryst. Liq. Cryst.* **1977**, *42*, 249. Bryan, R. F.; Forcier, P. G. *Mol. Cryst. Liq. Cryst.* **1980**, *60*, 133.

(26) Arora, S. L.; Fergason, J. L.; Taylor, T. R. *J. Org. Chem.* **1970**, *35*, 4055. Adams, J. M.; Morsi, S. E. *Acta Crystallogr., Sect. B* **1976**, *32*, 1345. Baumeister, V.; Harting, H.; Gdaniec, M.; Jaskolki, M. *Mol. Cryst. Liq. Cryst.* **1981**, *69*, 119. Haase, W.; Paulus, H.; Pendzialek, R. *Mol. Cryst. Liq. Cryst.* **1983**, *101*, 429.

(27) Bruce, D. W.; Dunmur, D. A.; Lalinde, E.; Maitlis, P. M.; Styring, P. *Liq. Cryst.* **1988**, *3*, 384.

(28) Wells, A. F. *Structural Inorganic Chemistry*; Oxford University Press: Oxford, 1984.

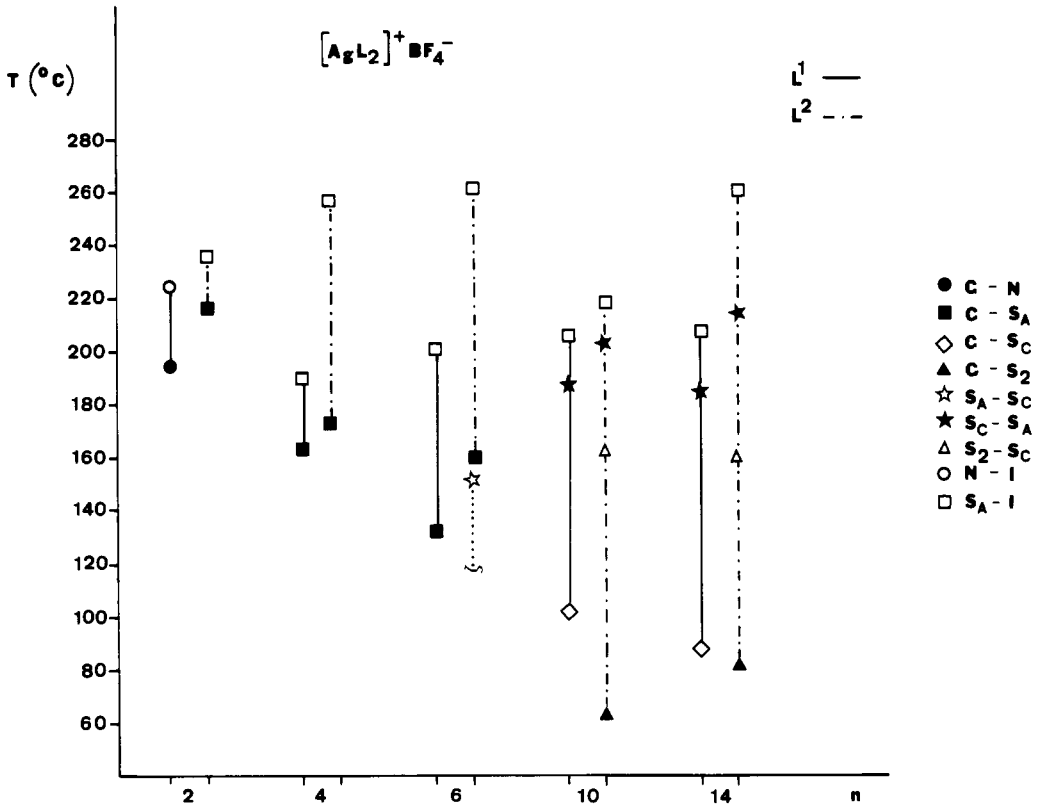


**Figure 10.** Comparative study of transition temperatures of liquid crystal complexes of $BF_4^-$ series.

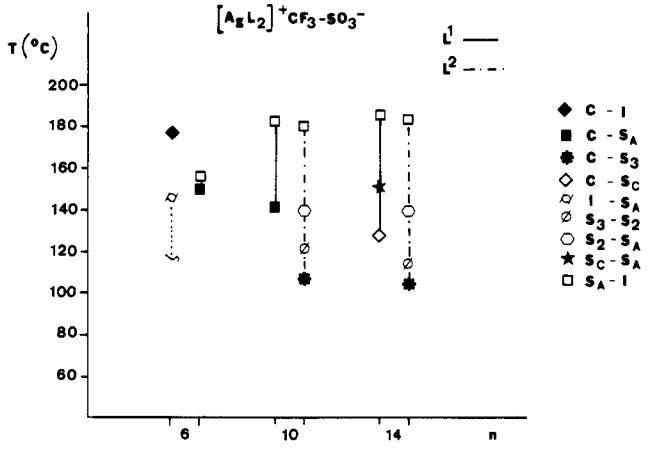


**Figure 11.** Comparative study of transition temperatures of liquid-crystal complexes of the $CF_3SO_3^-$ series.

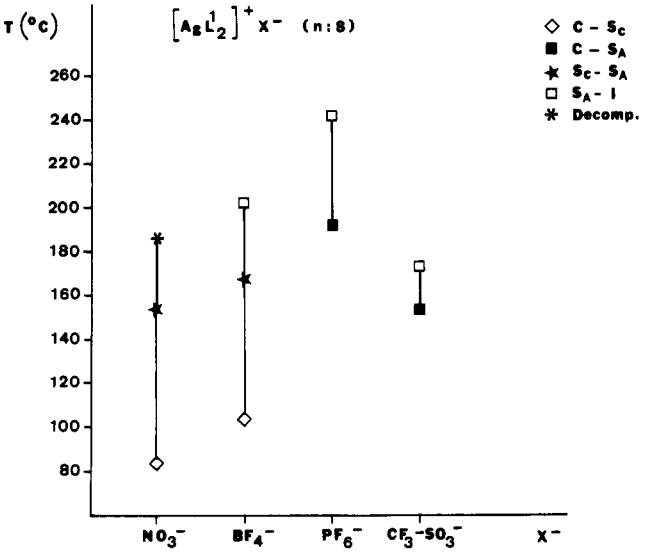


**Figure 12.** Comparative study of liquid-crystal properties of different (octyloxy)imine complexes of silver(I).

the mesomorphic properties. The change of the internal functional group in the organic ligand mainly affects both the mesophase range and the type of mesophase.

**X-ray Studies.** To obtain other experimental data in support of our previously mentioned proposals, X-ray diffraction experiments at the mesophase were performed with four compounds described in this paper: $[AgL^1_2]^+BF_4^-$, $[AgL^1_2]^+CF_3SO_3^-$ with $n = 8$ and $[AgL^2_2]^+BF_4^-$, $[AgL^2_2]^+CF_3SO_3^-$ with $n = 10$. Due to the instability of these silver complexes, only short-time experiments (5–10 min) could be carried out.

Low-angle reflections showed that in all these compounds, irrespective of the ligand, the layer thickness at the mesophase ($S_A$ and $S_C$) was 41–45 Å, shorter than the calculated fully extended molecule lengths of the imine and ester complexes 48 and 53 Å, respectively (as determined from Dreiding stereomodels). These differences are not unexpected because of the tilt of the long axes in the $S_C$ mesophase and because of thermal fluctuations[29,30] in the $S_A$ mesophase. Also conformational changes (partial melting of the long terminal chains) reduce the effective length in relation to the fully extended molecule length.[30]

It was difficult to determine the intermolecular lateral distances in the mesophase because we were unable to obtain sufficiently exposed diagrams that would have enabled us to see clearly the diffuse scattering at wide angles. However, in some diagrams a very diffuse halo could be seen at a scattering angle region similar to that generally found for the usual $S_A$ and $S_C$ mesophases ($2\vartheta$ about

(29) Leadbetter, A. J.; Frost, J.; Gaughan, J. P.; Mazid, M. A. *J. Phys. Colloque C-3* **1979**, *40*, C3-178.
(30) Bryan, R. F.; Leadbetter, A. J.; Mehta, A. I.; Tucker, P. A. *Mol. Cryst. Liq. Cryst.* **1984**, *104*, 257.

18-20°). The spreading of the halo prevents an accurate evaluation of the average lateral distance, and consequently we could not determine whether the ligand or the counterion influences these distances. Furthermore, scattering at wide angles is related to some average electron density distribution, which originates from different interferences (between silver atoms, paraffinic chains aromatic groups, counterions). The effect on the X-ray pattern of an eventual separation of the rigid cores of neighboring molecules would be masked by a higher degree of chain melting, as it is not possible to differentiate between the contribution of the chains and of the rest of the molecule to X-ray diffraction.

**Acknowledgment.** We express our appreciation to Dr. A. M. Levelut (Laboratoire de Physique des Solids, University Paris-Sud) for providing access to the X-ray equipment. Likewise, Dr. J. Barberá acknowledges a NATO grant. This work was supported by the EEC (Project ST2J-0387-C).

**Registry No.** $L^1$ ($n$ = 1), 129985-68-8; $L^1$ ($n$ = 2), 129985-69-9; $L^1$ ($n$ = 3), 129985-70-2; $L^1$ ($n$ = 4), 129985-71-3; $L^1$ ($n$ = 5), 129985-72-4; $L^1$ ($n$ = 6), 129985-73-5; $L^1$ ($n$ = 7), 129985-74-6; $L^1$ ($n$ = 8), 129985-75-7; $L^1$ ($n$ = 9), 129985-76-8; $L^1$ ($n$ = 10), 129985-77-9; $L^1$ ($n$ = 12), 129985-78-0; $L^1$ ($n$ = 14), 129985-79-1; $L^1$ ($n$ = 16), 129985-80-4; $L^2$ ($n$ = 2), 129985-81-5; $L^2$ ($n$ = 4), 129985-82-6; $L^2$ ($n$ = 6), 129985-83-7; $L^2$ ($n$ = 10), 129985-84-8; $L^2$ ($n$ = 14), 129985-85-9; $[AgL^1_2]^+BF_4^-$ ($n$ = 1), 130010-99-0; $[AgL^1_2]^+BF_4^-$ ($n$ = 2), 122676-75-9; $[AgL^1_2]^+BF_4^-$ ($n$ = 3), 130011-01-7; $[AgL^1_2]^+BF_4^-$ ($n$ = 4), 130011-03-9; $[AgL^1_2]^+BF_4^-$ ($n$ = 5), 130011-05-1; $[AgL^1_2]^+BF_4^-$ ($n$ = 6), 130011-07-3; $[AgL^1_2]^+BF_4^-$ ($n$ = 7), 130011-09-5; $[AgL^1_2]^+BF_4^-$ ($n$ = 8), 130011-11-9; $[AgL^1_2]^+BF_4^-$ ($n$ = 9), 130011-13-1; $[AgL^1_2]^+BF_4^-$ ($n$ = 10), 130011-15-3; $[AgL^1_2]^+BF_4^-$ ($n$ = 12), 130011-17-5; $[AgL^1_2]^+BF_4^-$ ($n$ = 14), 130031-55-9; $[AgL^1_2]^+BF_4^-$ ($n$ = 16), 130031-57-1; $[AgL^1_2]^+CF_3SO_3^-$ ($n$ = 5), 130011-18-6; $[AgL^1_2]^+CF_3SO_3^-$ ($n$ = 6), 130011-19-7; $[AgL^1_2]^+CF_3SO_3^-$ ($n$ = 7), 130011-20-0; $[AgL^1_2]^+CF_3SO_3^-$ ($n$ = 8), 130011-21-1; $[AgL^1_2]^+CF_3SO_3^-$ ($n$ = 9), 130011-22-2; $[AgL^1_2]^+CF_3SO_3^-$ ($n$ = 10), 130011-23-3; $[AgL^1_2]^+CF_3SO_3^-$ ($n$ = 12), 130011-24-4; $[AgL^1_2]^+CF_3SO_3^-$ ($n$ = 14), 130031-58-2; $[AgL^1_2]^+CF_3SO_3^-$ ($n$ = 16), 130031-59-3; $[AgL^2_2]^+BF_4^-$ ($n$ = 2), 130011-26-6; $[AgL^2_2]^+BF_4^-$ ($n$ = 4), 130011-28-8; $[AgL^2_2]^+BF_4^-$ ($n$ = 6), 130011-30-2; $[AgL^2_2]^+BF_4^-$ ($n$ = 10), 130011-32-4; $[AgL^2_2]^+BF_4^-$ ($n$ = 14), 130011-34-6; $[AgL^2_2]^+CF_3SO_3^-$ ($n$ = 4), 130011-35-7; $[AgL^2_2]^+CF_3SO_3^-$ ($n$ = 6), 130031-60-6; $[AgL^2_2]^+CF_3SO_3^-$ ($n$ = 10), 130011-36-8; $[AgL^2_2]^+CF_3SO_3^-$ ($n$ = 14), 130011-37-9; $[AgL^1_2]^+NO_3^-$ ($n$ = 6), 130011-38-0; $[AgL^1_2]^+PF_6^-$ ($n$ = 6), 130011-39-1.

# Low-Dimensional Organometallic Electron-Transfer Complexes. X-ray Structures and Magnetic Properties of $\alpha$- and $\beta$-$[Cr(C_6Me_3H_3)_2]^{\cdot+}[TCNQ]^{\cdot-}$

Dermot O'Hare,[1a] Michael D. Ward,*[,1b] and Joel S. Miller*

*Central Research and Development Department,† E. I. du Pont de Nemours and Company, Experimental Station E328, Wilmington, Delaware 19880-0328*

*Received May 14, 1990*

The reaction of donor, $Cr(arene)_2$ (arene = $C_6Me_6$ and $C_6Me_3H_3$), D, with the acceptor TCNQ, A, results in formation of electron-transfer salts of $[D]^{\cdot+}[A]^{\cdot-}$ composition. Two phases of $[Cr(C_6Me_3H_3)_2]^{\cdot+}[TCNQ]^{\cdot-}$ have been structurally characterized. The $\alpha$-phase belongs to the centrosymmetric $C2/c$ space group [$a$ = 14.014 (4) Å, $b$ = 16.347 (4) Å, $c$ = 22.964 (6) Å, $\beta$ = 107.44 (2)°, $Z$ = 8, $V$ = 5019 (5) Å$^3$, $T$ = 23 °C, $R$ = 0.082] with the solid-state structure consisting of $\cdots D^{\cdot+}D^{\cdot+}A_2^{2-}D^{\cdot+}D^{\cdot+}\cdots$ linear chains. Each $[TCNQ]^-$ in the $[TCNQ]_2^{2-}$ dimer is planar, and the intradimer separation is 3.47 Å. The anion–anion overlap is unusual as the dihedral angle between the planes normal to the long molecular axes is 31°. The $\beta$-phase crystallizes in the $P2_1/c$ space group [$a$ = 9.588 (5) Å, $b$ = 16.390 (3) Å, $c$ = 8.419 (6) Å, $\beta$ = 106.84 (6)°, $Z$ = 2, $V$ = 1266 (9) Å$^3$, $T$ = 23 °C, $R$ = 0.044] with the solid-state structure consisting of $\cdots D^{\cdot+}A^{\cdot-}D^{\cdot+}A^{\cdot-}\cdots$ linear chains. The magnetic susceptibility of $\alpha$-$[Cr(C_6Me_6)_2][TCNQ]$ obeys the Curie–Weiss law with an effective moment, $\mu_{eff}$, of 1.77 $\mu_B$ and $\theta$ of −0.1 K. This is consistent with the presence of a diamagnetic $[TCNQ]_2^{2-}$ dimer ($\nu$(C≡N) = 2156 m, 2175 s, and 2182 s cm$^{-1}$). In contrast, $[Cr(C_6Me_3H_3)_2][TCNQ]$ does not obey the Curie–Weiss law but can be fit to an expression that accounts for contributions from independent Curie spins for the cation and a thermally activated triplet state for the dimerized anions [$\Delta E$ = 315 K, 0.027 eV, 219 cm$^{-1}$, 0.44 kcal/mol].

## Introduction

Low-dimensional electron-transfer complexes frequently exhibit unusual optical and electrical properties.[2,3] Recently we reported unusual cooperative magnetic properties for several alternating donor/acceptor electron-transfer complexes.[4] For example, the reaction of $Fe(C_5Me_5)_2$ and TCNQ (TCNQ = 7,7,8,8-tetracyano-$p$-quinodimethane) gives three products varying in stoichiometry, conductivity, and magnetic properties. The 1-D mixed-stack phase comprising alternating $S = {}^1/_2$ $[Fe(C_5Me_5)_2]^{\cdot+}$ donors and $S = {}^1/_2$ $[TCNQ]^{\cdot-}$ acceptors,[5,6] i.e., $\cdots D^{\cdot+}A^{\cdot-}D^{\cdot+}A^{\cdot-}\cdots$, exhibits a field-dependent metamagnetic switching from an antiferromagnetic to a high moment behavior.[4,7] The structurally similar $[Fe(C_5Me_5)_2]^{\cdot+}[TCNE]^{\cdot-}$ (TCNE =

† Contribution no. 5402.

(1) Current address: (a) Department of Inorganic Chemistry, Oxford University, Oxford Oxford, 0X1 3QR, UK. (b) Department of Chemical Engineering and Materials Science, University of Minnesota, Minneapolis, MN 55455.

(2) See for example: *Extended Linear Chain Compounds*; Miller, J. S., Ed.; Plenum: New York; Vols. 1-3. Simon, J.; Andre', J. J. *Molecular Semiconductors*; Springer-Verlag: New York, 1985.

(3) For a detailed overview, see the proceedings of the recent series of international conferences: *Synth. Met.* **1988**, *27*; **1989**, *28*, 29 (Aldissi, M., Ed.); *Mol. Cryst. Liq. Cryst.* **1985**, *117-121* (Pecile, C.; Zerbi, G.; Bozio, R.; Girlando, A., Eds.); *J. Phys. (Paris) Collogue* **1983**, 44-C3 (Comes, R., Bernier, P., Andre', J. J., Rouxel, J., Eds.); *Mol. Cryst. Liq. Cryst.* **1981**, *77*, *79*, *82*, *83*, *85*; **1982**, *86* (Epstein, A. J., Conwell, E. M., Eds.); *Chem. Scr.* **1981**, *17* (Carneiro, K., Ed.); *Lect. Notes Phys.* **1979**, *95*, *96* (Bartsic, S., Bjelis, A., Cooper, J. R., Leontic, B. A., Eds.); *Ann. N.Y. Acad. Sci.* **1978**, *313* (Miller, J. S., Epstein, A. J., Eds.).

0897-4756/90/2802-0758$02.50/0 